Int J Legal Med (2013) 127:159–167
DOI 10.1007/s00414-012-0712-8

ORIGINAL ARTICLE

Temporal profiles of axonal injury following impact acceleration traumatic brain injury in rats—a comparative study with diffusion tensor imaging and morphological analysis

Shangxun Li · Yan Sun · Dai Shan · Bin Feng · Jingjun Xing · Yijie Duan · Jiapei Dai · Hao Lei · Yiwu Zhou

Received: 22 December 2011 / Accepted: 27 April 2012 / Published online: 10 May 2012

Abstract Traumatic axonal injury (TAI) plays a major role in the development of neurological impairments after traumatic brain injury (TBI), but it is commonly difficult to evaluate it precisely and early with conventional histological biomarkers, especially when the patients experience short-term survival after TBI. Diffusion tensor imaging (DTI) has shown some promise in detecting TAI, but longitudinal studies on the compromised white matter with DTI at early time points (≤72 h) following impact acceleration TBI are still absent. In the present study, rats were subjected to the Marmarou model and imaged with DTI at 3, 12, 24, and 72 h (n=5 each) post-injury. Using a region-of-interest-based approach, the regions of interest including the corpus callosum, bilateral external capsule, internal capsule, and pyramidal tract were studied. Two DTI parameters, fraction anisotropy and axial diffusivity, were significantly reduced from 3 to 72 h in each region after trauma, corresponding to the gradient of axonal damage demonstrated by immunohistochemical staining of β-amyloid precursor protein and neurofilament light chain. Remarkably, DTI changes predicted the approximate time in the acute phase following TBI. These results indicate that the temporal profiles of diffusion parameters in DTI may be able to provide a tool for early diagnosis of TAI following impact acceleration TBI.

Keywords Traumatic brain injury · Traumatic axonal injury · Diffusion tensor imaging · Biomarker · β-Amyloid precursor protein · Neurofilament

Abbreviations

TBI	Traumatic brain injury
TAI	Traumatic axonal injury
DTI	Diffusion tensor imaging
β-APP	β-Amyloid precursor protein
NF	Neurofilament
ARBs	Axonal retraction balls
AD	Axial diffusivity
FA	Fraction anisotropy
ADC	Apparent diffusion coefficient
RD	Radial diffusivity
ROIs	Regions of interest
CC	Corpus callosum
IC	Internal capsule
LIC	Left internal capsule
RIC	Right internal capsule

Electronic supplementary material The online version of this article (doi:10.1007/s00414-012-0712-8) contains supplementary material, which is available to authorized users.

S. Li · J. Xing · Y. Duan · Y. Zhou (✉)
Faculty of Forensic Medicine,
Tongji Medical College of Huazhong University of Science and Technology,
Wuhan 430030, China
e-mail: yiwuhedi@sina.com

Y. Sun · B. Feng · J. Dai (✉)
Wuhan Institute for Neuroscience and Neuroengineering,
South Central University for Nationalities,
Wuhan 430074, China
e-mail: jdai@mail.scuec.edu.cn

D. Shan · H. Lei (✉)
State Key Laboratory of Magnetic Resonance and Atomic and Molecular Physics, Wuhan Center for Magnetic Resonance,
Wuhan Institute of Physics and Mathematics,
Chinese Academy of Sciences,
Wuhan 430071, China
e-mail: leihao@wipm.ac.cn

EC	External capsule
LEC	Left external capsule
REC	Right external capsule
PY	Pyramidal tract
LPY	Left pyramidal tract
RPY	Right pyramidal tract
HP	Hippocampus
TBS	Tris-buffered saline

Introduction

Traumatic brain injury (TBI) is a leading cause of morbidity and mortality with an estimated 10 million people affected annually, being serious enough to result in hospitalization or death [1]. Traumatic axonal injury (TAI) is well known to be closely associated with TBI and thought to be a major contributor to neurological impairments following TBI [2, 3]. Although significant progresses have been made in understanding the pathophysiologic cascades involved in TAI [4, 5], the accurate identification of axonal injury remains a challenge in clinical and forensic sciences. So far, axonal injury has been characterized histologically using silver staining [6], horseradish peroxidase uptake [7], immunohistochemical staining of neurofilament (NF) [8, 9] and β-amyloid precursor protein (β-APP) [10, 11]. The increasing use of proteomic or degradomic techniques helps to examine large numbers of proteins from brain tissue of TAI animals or humans for either decreases in intact proteins or appearances of novel low-molecular-weight proteins that represent putative breakdown products [12], yielding feasibility of the detection of TAI in animals and humans. It has been verified that β-APP-stained axonal injury could be detected by 1.75 or 3 h after trauma in humans [13, 14]. However, it has also been suggested that TAI is more difficult to diagnose or quantify than the focal types of TBI since the macroscopic abnormalities are commonly minimal. In addition, the microscopic lesions are not specific to TAI and are sometimes not apparent when the survival period is short [15]. Moreover, it is sometimes difficult to make an early diagnosis by using a single biomarker related to only one type of injured constituent due to the multiple elements contributing to axotomy. Hence, it is imperative to identify TAI by the combination of different biomarkers that could reflect the multiple mechanisms of TAI.

Recently, advances in neuroimaging and laboratory techniques have allowed for more subtle lesions to be detected earlier, potentially allowing the early diagnosis of TAI. Diffusion tensor imaging (DTI) has shown some advantages for detecting axonal injury by acquiring water diffusion in different directions to provide microstructural information about axons or myelin [16–19]. The directional diffusivities include three principle eigenvalues: axial diffusivity (AD; λ_1 or $\lambda_\parallel$), λ_2, λ_3, as well as several derivative parameters consisting of fraction anisotropy (FA), relative anisotropy (RA), radial diffusivity (RD; $\lambda_\perp = (\lambda_2 + \lambda_3) / 2$), and apparent diffusion coefficient (ADC = $(\lambda_1 + \lambda_2 + \lambda_3) / 3$). DTI has been employed in detecting white matter pathology in experimental animal models including demyelinating diseases [20], multiple sclerosis [21], and traumatic spinal cord injury [22, 23]. Recently, the correlations between diffusion parameters and immunolabeled axons have been established in experimental controlled cortical impact injury [24, 25], typically in pericontusional white matter tracts. To our knowledge, none of the previous animal studies has performed DTI at multiple acute time points in impact acceleration TBI. Moreover, the sensitivity and specificity of DTI towards axonal injury in the brainstem have not been studied yet.

In the present study, we hypothesized that the changes of the diffusivities seen in DTI images would correspond to TAI verified histologically within the selected regions of interest (ROIs) of the white matter including the corpus callosum (CC), bilateral internal capsule (IC), external capsule (EC), and pyramidal tract (PY) in rats following impact acceleration TBI and that the DTI signal changes could approximately distinguish the time during the acute phase post-TBI.

Materials and methods

Experimental TBI: impact acceleration brain injury

All procedures were approved by the guidelines for the care and use of animals in China. Twenty-five male Sprague-Dawley rats weighing 200–250 g were used. General anesthesia was induced by intraperitoneal (i.p.) injection with 10 % chloral hydrate at 0.3 ml/100 g body weight. Impact acceleration TBI was induced according to previous reports [26, 27]. Briefly, following a midline incision between coronal and lambdoid sutures, a steel disk 10 mm in diameter and 3 mm thick was adhered to the skull between the bregma and lambda suture. Then, the animal was placed on a foam bed in the prone position and fastened by a belt around the trunk, with the disk centered right under the lower end of a 1 m plexiglass tube. A cylindrical steel weight of 450 g was allowed to fall through the tube at a designated height of 1 m to impact the disk. Then, the rat was immediately removed and the scalp was sutured after gently removing the steel disk from the skull. In the sham group, rats underwent the surgical procedure without impact. Animals were imaged with DTI at the desired time points at 3, 12, 24, and 72 h after impact acceleration brain injury (n=5 for each time point).

DTI scanning

For DTI scanning, rats were deeply anesthetized with 10 % urethane (1.2 g/kg, i.p.) to prevent the disturbance of unstable breath and circulation during DTI scanning, then rats were placed in a magnetic resonance-compatible stereotaxic frame of a 7.0-T/20 cm Bruker Biospec scanner (Karlsruhe, Germany) with a 72 mm diameter volume coil for radio frequency transmission and a quadrature surface coil for signal detection. Body temperature was maintained at 37°C by heated circulating water, and respiration was monitored by detecting the chest motion of the animal with two fiber optic cables and the signal was fed into an oscilloscope that monitored the chest motion throughout the scanning. To obtain anatomically matched coronal image slices at each time point, identical anatomical landmarks were used to center and align the brain in each image plane.

A spin-echo echo-planar DTI sequence was used with the following acquisition parameters: repetition period (TR) of 5,000.001 ms, echo time (TE) of 26 ms, flip angle of 90°, time between application of gradient pulses (Δ) of 14 ms, diffusion gradient duration (δ) of 3 ms, slice thickness of 0.8 mm, slice interval of 0 mm, field of view of 30×30 mm^2, and matrix size of 128×128 (zero filled to 256×256). Diffusion-sensitizing gradients were applied along 30 directions. The *b* value used for the acquisition of diffusion-weighted images was 800 s/mm^2. The nominal voxel size was 117×117×800 μm after zero filling. The scanning area was set ranging from the genu of CC to the end of medulla oblongata, and the total imaging time was about 46 min 40 s 0 ms.

Analysis of DTI images using anatomically defined ROIs

Using a region-of-interest-based approach, DTI parameters (λ_1, λ_2, λ_3, FA, and ADC) were acquired from the CC, IC, EC, and PY through 20 coronal slices for the image sets with the same anatomical landmark-based rules. FA images were used for outlining the ROIs. The image software (Paravision 5.0) binding feature allowed for the replication of the traced ROI to other images. Similar to the definition in the previous studies of mouse [24, 25], the boundaries of the CC and EC in rats were defined as follows: in the most rostral regions (bregma +1.60 to −0.92 mm), the boundary was the lateral edge of the cingulum; in the regions (bregma −0.92 to −2.80 mm), the boundary of the CC was defined by a horizontal line extending laterally from the bottom of the fimbria until it intersected with the EC; moving more caudally (bregma −2.80 to −5.30 mm) [28], a horizontal line extending laterally from the lateral-inferior edge of the hippocampus (HP) was employed. Bilateral IC (bregma −0.26 to −4.52 mm) and PY (bregma −8.3 to −14.08 mm) were also well outlined. The program then returned the mean signal intensity for each traced ROI on each slice. Overall, for each diffusion parameter in each animal, five values of CC and EC, four values of IC, and seven values of PY were obtained. We verified that all chosen anatomical landmarks were clearly visible in FA images, and the observer was blind to the cases during the delineation of the ROIs. Moreover, a portion of the images were retraced 15 days after the first tracing. All parameters were compared between the first and second tracings. No significant differences were found in the ROI tracing method. It could be concluded that the ROI tracing method did not add significant variance.

To establish the correlations between the DTI parameters and immunochemical profiles, changes in AD and FA were expressed using normalized AD and FA as in previous studies [24, 25]. They were calculated by dividing the AD or FA in the injured ROI by the mean AD or FA in the corresponding ROI from the control group.

Histology

Immediately after imaging, the rats were transcardially perfused with 0.9 % saline+0.3 % heparin, followed by perfusion with 4 % paraformaldehyde. Then, the brains were removed and immersed in the same fixative overnight (16–18 h). The cerebrum and brainstem were obtained using two transverse cuts: the first at the level of the inferior colliculus within the midbrain region and the second 2 mm caudal to the pyramidal decussation within the medulla oblongata [27, 29]. The brainstem was then divided equally by a sagittal cut to include the basal interpeduncular regions of the brain, pons, and pyramids inclusive of the left pyramidal tract (LPY) and right pyramidal tract (RPY) areas where high densities of traumatically injured axons have previously been described utilizing the Marmarou model [27, 29]. The cerebral blocks were trimmed to contain the complete CC. The blocks were then immersed in 30 % sucrose for further tissue processing. To strictly distinguish the side of slices, serial coronal sections of the cerebrum and serial sagittal sections from the midline to lateral of bilateral brainstem blocks were cut on a freezing microtome (CM3050S, Leica) with the thickness of 30 μm and mounted on gelatin-covered microscope slides. Every sixth section was used for histology. For each block of the unilateral brainstem, 36 sections were obtained as the width of the unilateral PY is about 1.2 mm.

The sections were washed three times in Tris-buffered saline (TBS) (pH=7.6) for 5 min each. After incubation with 0.3 % H_2O_2 in TBS for 30 min at room temperature, the sections were rinsed in TBS three times for 10 min each. Then, the sections were incubated with either rabbit monoclonal anti-β-APP antibody (Y188, 1:200, Abcam, Cambridge, UK) or mouse monoclonal anti-68-kD neurofilament (NF-L) antibody (NR4, 1:200, Sigma, St. Louis,

MO, USA) overnight at 4°C. The following day, the sections were washed three times in TBS for 10 min each, followed by the incubation with biotinylated secondary goat antirabbit IgG (for β-APP) or goat antimouse IgM (for NF-L) for 1 h at room temperature in a 1:400 dilution (Boster Biological Technology, Ltd., Wuhan, China). Thereafter, the sections were washed three times in TBS for 5 min each. Incubated with ABC Elite (Vector Laboratories, Inc., Burlingame, CA, USA) at a 1:400 dilution in TBS for 2 h at room temperature, the sections were washed with TBS three times for 5 min each and developed with 3,3′-diaminobenzidine tablets (Boster Biological Technology, Ltd., Wuhan, China). Final three TBS washes were performed for 10 min each. The sections were allowed to dry and dipped for 5 min each in 50–75–90–95–95–100–100 % ethanol solutions, followed by two treatments for 10 min each in xylene. Finally, the sections were coverslipped. To control for possible cross-reaction between the first primary antibody and the second secondary antibody, the first or second primary antibodies were omitted. In this condition, no staining was observed.

Analysis of axonal injury as defined by APP and NF-L immunostaining in the ROIs

All immunostained sections were examined under Nikon Eclipse 90i microscope (Tokyo, Japan). A quantitative method was employed to quantify the numbers of APP-stained axons per square millimeter in the ROIs, including axonal deposits, swelling, and bulbs. The ROI was outlined in each section at low magnification (×40) and followed by systematic counts of individual injured axons at high magnification (×200). The observer was blind to the cases. Red blood cells and other non-axonal stained structures were not counted. Then, the numbers of APP-stained axonal varicosities per square millimeter were obtained by dividing the counts of injured axons by the area of each sampled region generated by the software. Due to the peculiar pattern of NF-L immunostaining (see the "Results" and "Discussion" sections), the mean density of NF-L immunostaining was employed to evaluate the degree of axonal damage.

Statistical methods

All data were analyzed using IBM SPSS Statistics 17.0. There were no prespecified hypotheses about the histological or DTI parameters between the left and right side of the IC, EC, or PY at each time point, so a two-tailed *t* test was used. The threshold for statistical significance was set to $P<0.05$ without correction for multiple comparisons. For the comparisons of immunostaining profiles or DTI diffusion parameters between different groups, a one-way analysis of variance (ANOVA) was used followed by a Fisher post hoc test to correct for multiple comparisons.

Results

Histochemical findings

No APP-stained axons were found in each ROI of the control animals, as well as in bilateral IC and EC in the injured animals. Spatial differences and temporal gradient of axonal injury were observed in the injured groups. APP staining was substantially obvious in the PY, posterior body, and splenium of the CC in the injured animals. Oblong and round APP-stained varicosities were noticed under high magnification (Fig. 1). At 3 h after injury, APP antibody-

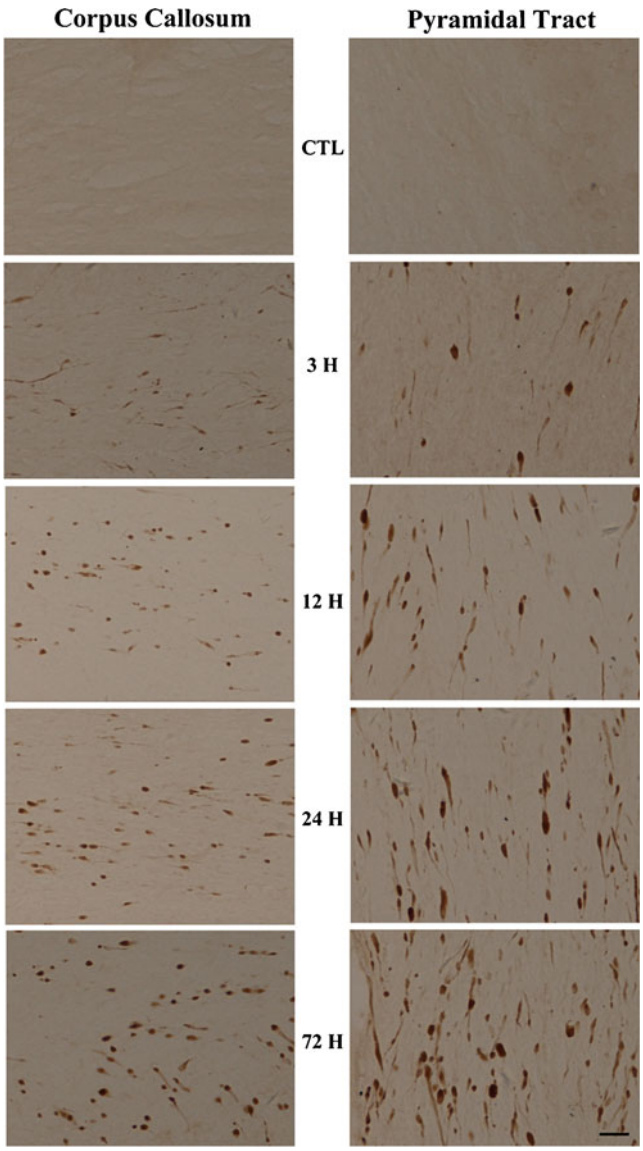

Fig.1 Axonal injury detected by APP staining following impact acceleration TBI. Uninjured tissue (*CTL*) shows no APP staining. Acutely after injury, numerous APP-stained axons were found in the CC and PY. Immunoreactive profiles in these regions markedly increased in size and number over time, including axonal swellings and ARBs (scale bar = 50 μm)

labeled axonal deposits mainly presented as dot-like profiles. At 12–72 h post-injury, the immunoreactive profiles including axonal swellings and axonal retraction balls (ARBs) markedly increased in size and number in the ROIs. Significant increases in the numbers of APP-stained axonal varicosities were observed in the CC and bilateral PY over time after injury (Fig. 2).

For further verification of axonal damage, the brain sections were stained with the anti-neurofilament light chain antibody, NF-L. In the control group, there was no NF-L staining in the CC, EC, and IC, with the exception of the PY, which presented weak positive staining. While in the injured groups, diffuse staining with increasing density over time was observed in each ROI. Moreover, several axonal swellings were also seen in the CC and PY since 3 h post-TBI (Supplemental Fig. 1). The mean density of the NF-L staining increased congruously after injury in each ROI, with a sharp increase from 3 to 24 h and a slight increase at 72 h (Supplemental Fig. 2). Overall, the two markers of axonal damage revealed similar temporal trends, with significantly increased immunostaining from 3 to 72 h in the ROIs (Fig. 2 and Supplemental Fig. 2).

DTI analysis

The anatomical extent of the ROIs was used for DTI analysis. An example (Supplemental Fig. 3) indicates the lateral-inferior edge of the HP, which was used as the boundary of the CC and EC. To display the grayscale changes clearly, the imaging modalities were trimmed to contain one half of the CC, the right external capsule (REC), and right internal capsule (RIC) in the coronal views. Another example is provided for demonstrating the changes of FA in bilateral

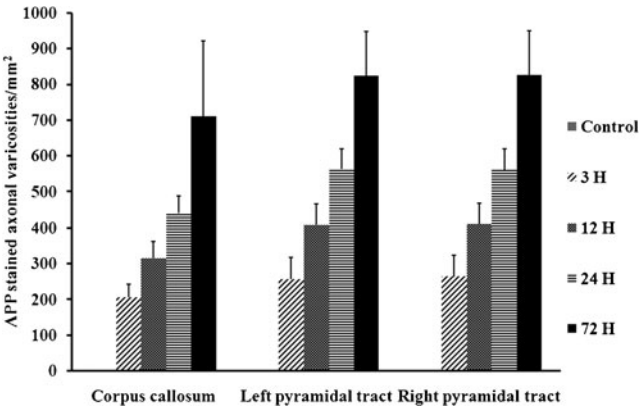

Fig.2 Estimated numbers of APP-stained axonal varicosities per square millimeter as a function of time after injury. There were statistically significant increases in APP-stained axonal varicosities in the CC and bilateral PY at all time points after trauma, with the highest numbers at 72 h (one-way ANOVA, $P<0.05$). Moreover, no differences were found between bilateral PY at each time point (two-tailed t test, $P>0.05$). $n=5$ rats per group. *Error bars* denote standard deviations

PY (Supplemental Fig. 4). The CC and PY in the control images had high FA, as expected for a highly organized tissue. Acutely after injury, there were dramatic reductions of signals in FA in the CC and PY in the post-TBI images. The gradient of reduced signal of FA was also visible in these images. For AD and ADC images, no apparent grayscale changes were seen in the PY (data not shown) and decreased signal intensities were only seen at 3 h in the CC, while the remaining imaging modalities showed no visible grayscale changes. In addition, no visible grayscale changes were seen in the three parameters in the REC and RIC. As to the images of λ_2 and λ_3 of the ROIs, no visible changes were noted (data not shown).

A quantitative analysis of DTI parameters within the ROIs was performed (Supplemental Fig. 5). The AD and FA in each ROI were significantly reduced after injury compared with the control. Multiple comparisons showed that they also decreased consistently over time in each ROI (Supplemental Fig. 5a, b). Namely, the AD and FA were consistently decreased over time in acute phase post-TBI, and the injured groups could be approximately separated from each other by using the two parameters. There were consistently decreased ADC over time in bilateral IC and EC in injured groups, whereas in the CC and bilateral PY, ADC decreased congruously before 24 h, but there were no differences between 24 and 72 h (Supplemental Fig. 5c). For RD, it did not change consistently over time (Supplemental Fig. 5d). However, with multiple comparisons, a slightly increased RD was found in the CC since 24 h, but it was only elevated at 72 h in bilateral IC, EC, and PY. Accordingly, of the diffusion parameters evaluated, only AD and FA permitted a complete separation between injured and uninjured rats.

No significant differences in the number of APP-stained axonal varicosities, mean density of NF-L, or diffusion diffusivities were found between the left and right side of the IC, EC, or PY at each time point (data not shown).

The relationship between the histochemical findings and DTI analysis

The changes in DTI parameters were correlated with the numbers of APP-immunostained axons in the CC and bilateral PY and the mean density of NF-L staining in each ROI. There were better correlations between the changes of FA and the numbers of APP-stained axons in the CC (Fig. 3a; $P<0.05$, $R^2=0.762$), the LPY (Fig. 3b; $P<0.05$, $R^2=0.833$), and the RPY (Fig. 3c; $P<0.05$, $R^2=0.877$). The correlations between the normalized AD and APP-stained axons were also significant in the CC, LPY, and RPY (Fig. 3d–f; $P<0.05$, $R^2=0.735$, 0.815, and 0.857). Significant correlations were also found between the changes in FA or AD and the mean density of NF-L in each ROI. The R^2 of

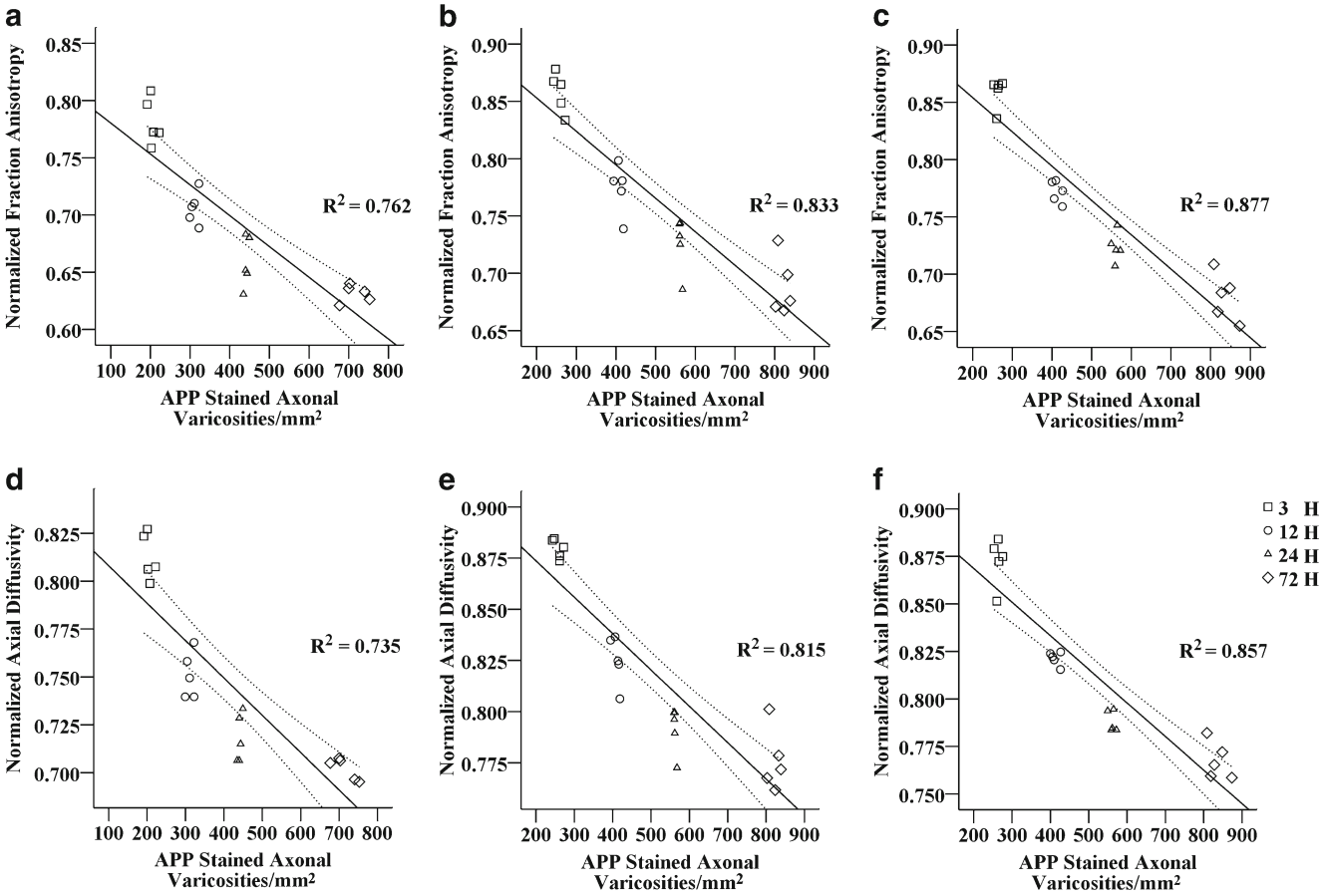

Fig.3 Quantitative correlations between the DTI parameters and the numbers of injured axons as demonstrated with APP immunohistochemistry. **a**–**c** Correlations of normalized FA with the estimated numbers of APP-stained axons per square millimeter in the CC, LPY, and RPY ($P<0.05$). **d**–**f** Correlations of normalized AD with the estimated numbers of APP-stained axons per square millimeter in the CC, LPY, and RPY ($P<0.05$). Each symbol represents a single rat at one time point. The values of DTI parameters of injured animals were normalized by dividing by the mean values of the same ROI in the uninjured rats. Estimates of the number of APP-stained axons per square millimeter were obtained by dividing the total number of counted APP-stained axonal varicosities by the total area of the counted sampling zones. Better correlations were found between the change in FA and the severity of axonal injury as defined with APP immunostaining. *Dashed lines* represent the 95 % confidence band

normalized FA and the mean density of NF-L staining in the CC, LPY, RPY, left internal capsule (LIC), RIC, left external capsule (LEC), and REC was 0.847, 0.738, 0.849, 0.707, 0.627, 0.802, and 0.849, respectively (Supplemental Fig. 6a–g). While the R^2 of normalized AD and the mean density of NF-L staining in the CC, LPY, RPY, LIC, RIC, LEC, and REC was 0.838, 0.743, 0.844, 0.787, 0.687, 0.838, and 0.902, respectively (Supplemental Fig. 6h–n). The data were tightly clustered around the regression line, such that the 95 % confidence bands were narrow.

Discussion

In the present study, with the combination of DTI and morphological observations, we carried out a comparative analysis of temporal profiles of axonal injury following impact acceleration TBI in rats. We found that the changes detected by DTI in the ROIs such as the CC, IC, EC, and PY could be verified with immunohistochemical staining for APP and NF-L, the two markers of axonal damage, suggesting that DTI is not only able to distinguish injured white matter from uninjured white matter but also offers the approximate information on the timing of acute axonal injury (≤72 h).

As the most classic and practical impact acceleration brain injury model for producing TAI with relative minor neuronal and vascular damage in the brain parenchyma, the Marmarou model was used in the current investigation. It has well demonstrated the imitation of human TBI and reproducible widespread and massive axonal injury [30, 31], which is mainly located in the CC, IC, optic tracts, cerebral and cerebellar peduncles, and long tracts in the brainstem [27]; accordingly, ROIs including the CC, IC, and PY as well as the EC were selected to be studied. It has been pointed out that the inadequacies encountered with

this model should not be discarded, including the lack of precise control over biomechanics, potential lateralization, or uneven distribution of the impact [30, 31]; hence, the IC, EC, and PY were observed bilaterally to evaluate the latent biomechanics defects in this study.

In animal models of TAI, β-APP accumulates rapidly and massively in damaged axons [32], and the antibody against β-APP labels injured axons as early as 2 to 6 h post trauma in rats, including waving, varicose axons and ARBs [33, 34]. NF-L is the first subunit to be degraded into fragments and is inevitable to the increasing immunoactivity to be detected at an early stage and proved to be the most sensitive and specific biomarker for the detection of injured axons [35–37]. In the present study, the time windows and regional distribution for β-APP-positive immunostaining are correlated well with previous experimental studies [29, 38–40]. Primarily, it is prominently located in the parasagittal projection fiber tracts and transverse fiber tracts particularly in the midline structures of the brain including caudal parts of the CC and brainstem. Indeed, it is noticeable that no axonal damage in the IC and EC was observed with APP staining; these may be attributed to the reason that APP selectively labels injured axons regularly oriented or scattered irregularly along the white matter bundles, the feeble effect in these areas relative far away from the impact epicenter, and the mild degree of TAI in the deep white matter defined with APP immunostaining. The patterns of NF-L staining were also accorded with the previous findings [8, 9, 29, 41], but presented some differences compared to that of APP staining. The NF-L profiles overcame the shortage of APP immunostaining towards the verification of mild axonal damage in the IC and EC by both diffuse axonal staining and focal axonal swellings staining in the ROIs. It has been shown that ARBs consist of a rim of β-APP, and a core of NF compaction contained highly disorganized cytoskeletal constituents that are devoid of NF immunoreactivity, contributing to fewer varicosities demonstrated by NF-L staining in the involved white matter compared to APP immunostaining. Consequently, the mean density of NF-L was preferentially selected and employed for evaluating the extent of axonal damage.

The persistent decreasing of diffusion along the axons over time was in accord with the corresponding increased APP or NF-L immunoreactivities, and the biophysics mechanisms are related to the impeded intracellular diffusion caused by severed axons reseal, as well as restrained extracellular diffusion resulted from large axonal varicosities or ARBs that compressed the extracellular spaces around axons [42]. The observed decreases in FA were due to either isolated reductions in AD at each time point or the combination of reduced AD and increased RD at certain time points. This differentiation was possible because of the predominant axonal injury at 3–12 h and the compromised axolemma and/or myelin sheath at 24 and/or 72 h, leading to the slightly increased diffusion perpendicular to the axons. Noticeably, water diffusion in biological tissue is also highly dependent on the ratio of extracellular to intracellular space, the decreased ADC values reflect intracellular edema (cytotoxic edema), and the increased ADC values correspond to an increase in the extracellular space (vasogenic edema). Highly mobile extracellular water shifts into the intracellular compartment, generating cytotoxic edema during the early stage of TBI, giving rise to the decreased ADC in our observations. Other factors affecting the shape of ADC include the density of fibers, the average diameter and directional similarity of fibers in the ROIs, and the degree of myelination [43]. Thus, the changes of ADC were more complex than other parameters. As this study concerned about the evidences between DTI signals with histologically confirmed axonal injury, concomitant edema type and pathologies that occurred in axolemma or myelin sheath such as demyelination and inflammation were discarded. And, the descriptions of these constituents may help in addressing the histological correlates of an isolated reduction in AD versus a decrease in AD with a concomitant increase in RD or the changes of ADC in TAI, as presented previously [25].

Importantly, animal trauma models tend to replicate only single factors involved in the pathobiology of TBI, and the present results were obtained from animal experiments with controlled experimental conditions. Whereas human TBI is a highly complex multifactorial disorder with variable TAI [31], the simplicity and inherent inability of animal models may underlie the discrepancy between experimental trials and clinical applications of DTI. Clinically, although significant progresses have been achieved in the diagnosis, treatment guidelines, and prognostic evaluation of TAI [16–18, 44, 45], the relationship between DTI findings and functional status remain largely matters of speculation and the potential emerging disturbances of abnormal signals caused by other neurologic and neuropsychiatric conditions must be regarded [46]. Accordingly, the relationships between DTI and histological findings in TAI that were established in animals should be treated with caution when applied in humans.

In conclusion, temporal profiles of diffusion parameters in rats following impact acceleration TBI can be associated with the gradient of axonal injury that were verified histologically, supporting that DTI may serve as a tool to assist in early evaluation of TAI. However, different injury degrees are needed to delineate the ability of DTI to accurately track the progression of TAI. Hence, further work is particularly desired to define and validate the utility of this approach.

Acknowledgments This work was supported by the Scientific Research Foundation for the Returned Overseas Chinese Scholars from State Education Ministry and the National Natural Science Foundation of China (Grant Nos. 30870674, 20921004, and 31070961) and partly by the Research Foundation for the Key Laboratory of Neuroscience and Neuroengineering from South Central University for Nationalities (XJS09001).

Conflict of interest All authors declare no conflicts of interest.

References

1. Hyder AA, Wunderlich CA, Puvanachandra P, Gururaj G, Kobusingye OC (2007) The impact of traumatic brain injuries: a global perspective. Neuro Rehabilitation 22:341–353
2. Adams JH (1982) Diffuse axonal injury in non-missile head injury. Injury 13:444–445
3. Medana IM, Esiri MM (2003) Axonal damage: a key predictor of outcome in human CNS diseases. Brain 126:515–530
4. Büki A, Povlishock JT (2006) All roads lead to disconnection?—Traumatic axonal injury revisited. Acta Neurochir (Wien) 148:181–194
5. Povlishock JT, Katz DI (2005) Update of neuropathology and neurological recovery after traumatic brain injury. J Head Trauma Rehabil 20:76–94
6. Strich SJ (1961) Shearing of nerve fibres as cause of brain damage due to head injury. Lancet 2:443–448
7. Povlishock JT, Becker DP, Cheng CL, Vaughan GW (1983) Axonal change in minor head injury. J Neuropathol Exp Neurol 42:225–242
8. Christman CW, Grady MS, Walker SA, Holloway KL, Povlishock JT (1994) Ultrastructural studies of diffuse axonal injury in humans. J Neurotrauma 11:173–186
9. Yaghmai A, Povlishock J (1992) Traumatically induced reactive change as visualized through the use of monoclonal antibodies targeted to neurofilament subunits. J Neuropathol Exp Neurol 51:158–176
10. Smith DH, Chen XH, Iwata A, Graham DI (2003) Amyloid beta accumulation in axons after traumatic brain injury in humans. J Neurosurg 98:1072–1077
11. Hayashi T, Ago K, Ago M, Ogata M (2009) Two patterns of beta-amyloid precursor protein (APP) immunoreactivity in cases of blunt head injury. Leg Med (Tokyo) 11 Suppl 1:S171-S173
12. Saatman KE, Creed J, Raghupathi R (2010) Calpain as a therapeutic target in traumatic brain injury. Neurotherapeutics 7:31–42
13. Blumbergs PC, Scott G, Manavis J, Wainwright H, Simpson DA, McLean AJ (1995) Topography of axonal injury as defined by amyloid precursor protein and the sector scoring method in mild and severe closed head injury. J Neurotrauma 12:565–572
14. Oehmichen M, Meissner C, Schmidt V, Pedal I, König HG (1999) Pontine axonal injury after brain trauma and nontraumatic hypoxic–ischemic brain damage. Int J Legal Med 112:261–267
15. Ogata M (2007) Early diagnosis of diffuse brain damage resulting from a blunt head injury. Leg Med (Tokyo) 9:105–108
16. Neil J, Miller J, Mukherjee P, Hüppi PS (2002) Diffusion tensor imaging of normal and injured developing human brain—a technical review. NMR Biomed 15:543–552
17. Sundgren PC, Dong Q, Gómez-Hassan D, Mukherji SK, Maly P, Welsh R (2004) Diffusion tensor imaging of the brain: review of clinical applications. Neuroradiology 46:339–350
18. Huisman TA, Schwamm LH, Schaefer PW, Koroshetz WJ, Shetty-Alva N, Ozsunar Y, Wu O, Sorensen AG (2004) Diffusion tensor imaging as potential biomarker of white matter injury in diffuse axonal injury. AJNR Am J Neuroradiol 25:370–376
19. Mori S, Zhang J (2006) Principles of diffusion tensor imaging and its applications to basic neuroscience research. Neuron 51:527–539
20. Song SK, Yoshino J, Le TQ, Lin SJ, Sun SW, Cross AH, Armstrong RC (2005) Demyelination increases radial diffusivity in corpus callosum of rat brain. NeuroImage 26:132–140
21. Kim JH, Budde MD, Liang HF, Klein RS, Russell JH, Cross AH, Song SK (2006) Detecting axon damage in spinal cord from a rat model of multiple sclerosis. Neurobiol Dis 21:626–632
22. Deo AA, Grill RJ, Hasan KM, Narayana PA (2006) In vivo serial diffusion tensor imaging of experimental spinal cord injury. J Neurosci Res 83:801–810
23. Nevo U, Hauben E, Yoles E, Agranov E, Akselrod S, Schwartz M, Neeman M (2001) Diffusion anisotropy MRI for quantitative assessment of recovery in injured rat spinal cord. Magn Reson Med 45:1–9
24. Mac Donald CL, Dikranian K, Song SK, Bayly PV, Holtzman DM, Brody DL (2007) Detection of traumatic axonal injury with diffusion tensor imaging in a rat model of traumatic brain injury. Exp Neurol 205:116–131
25. Mac Donald CL, Dikranian K, Bayly P, Holtzman D, Brody D (2007) Diffusion tensor imaging reliably detects experimental traumatic axonal injury and indicates approximate time of injury. J Neurosci 27:11869–11876
26. Marmarou A, Foda MA, van den Brink W, Campbell J, Kita H, Demetriadou K (1994) A new model of diffuse brain injury in rats. Part I: pathophysiology and biomechanics. J Neurosurg 80:291–300
27. Foda MA, Marmarou A (1994) A new model of diffuse brain injury in rats. Part II: morphological characterization. J Neurosurg 80:301–313
28. Paxinos G, Watson C (1997) The rat brain in stereotaxic coordinates. Elsevier, Amsterdam
29. Marmarou CR, Walker SA, Davis CL, Povlishock JT (2005) Quantitative analysis of the relationship between intra-axonal neurofilament compaction and impaired axonal transport following diffuse traumatic brain injury. J Neurotrauma 22:1066–1080
30. Wang HC, Ma YB (2010) Experimental models of traumatic brain injury. J Clin Neurosci 17:157–162
31. Cernak I (2005) Animal models of head trauma. NeuroRx 2:410–422
32. Smith DH, Meaney DF, Shull WH (2003) Diffuse axonal injury in head trauma. J Head Trauma Rehabil 18:307–316
33. Farkas O, Tamás A, Zsombok A, Reglodi D, Pál J, Büki A, Lengvári I, Povlishock JT, Dóczi T (2004) Effects of pituitary adenylate cyclase activating polypeptide in a rat model of traumatic brain injury. Regul Pept 123:69–75
34. Adelson PD, Jenkins LW, Hamilton RL, Robichaud P, Tran MP, Kochanek PM (2001) Histopathologic response of the immature rat to diffuse traumatic brain injury. J Neurotrauma 18:967–976
35. Serbest G, Burkhardt MF, Siman R, Raghupathi R, Saatman KE (2007) Temporal profiles of cytoskeletal protein loss following traumatic axonal injury in mice. Neurochem Res 32:2006–2014
36. Chen XH, Meaney DF, Xu BN, Nonaka M, McIntosh TK, Wolf JA, Saatman KE, Smith DH (1999) Evolution of neurofilament subtype accumulation in axons following diffuse brain injury in the pig. J Neuropathol Exp Neurol 58:588–596
37. Li J, Li XY, Feng DF, Pan DC (2010) Biomarkers associated with diffuse traumatic axonal injury: exploring pathogenesis, early diagnosis, and prognosis. J Trauma 69:1610–1618
38. Stone JR, Singleton RH, Povlishock JT (2001) Intra-axonal neurofilament compaction does not evoke local axonal swelling in all traumatically injured axons. Exp Neurol 172:320–331
39. Singleton RH, Stone JR, Okonkwo DO, Pellicane AJ, Povlishock JT (2001) The immunophilin ligand FK506 attenuates axonal injury in an impact-acceleration model of traumatic brain injury. J Neurotrauma 18:607–614
40. Gentleman SM, Nash MJ, Sweeting CJ, Graham DI, Roberts GW (1993) Beta-amyloid precursor protein (beta APP) as a marker for axonal injury after head injury. Neurosci Lett 160:139–144
41. Marmarou CR, Povlishock JT (2006) Administration of the immunophilin ligand FK506 differentially attenuates neurofilament

compaction and impaired axonal transport in injured axons following diffuse traumatic brain injury. Exp Neurol 197:353–362
42. Kraus MF, Susmaras T, Caughlin BP, Walker CJ, Sweeney JA, Little DM (2007) White matter integrity and cognition in chronic traumatic brain injury: a diffusion tensor imaging study. Brain 130:2508–2519
43. Westin CF, Maier SE, Mamata H, Nabavi A, Jolesz FA, Kikinis R (2002) Processing and visualization for diffusion tensor MRI. Med Image Anal 6:93–108
44. Newcombe VF, Williams GB, Nortje J, Bradley PG, Harding SG, Smielewski P, Coles JP, Maiya B, Gillard JH, Hutchinson PJ, Pickard JD, Carpenter TA, Menon DK (2007) Analysis of acute traumatic axonal injury using diffusion tensor imaging. Br J Neurosurg 21:340–348
45. Marquez de la Plata CD, Yang FG, Wang JY, Krishnan K, Bakhadirov K, Paliotta C, Aslan S, Devous MD, Moore C, Harper C, McColl R, Munro Cullum C, Diaz-Arrastia R (2010) Diffusion tensor imaging biomarkers for traumatic axonal injury: analysis of three analytic methods. J Int Neuropsychol Soc 17:24–35
46. Wortzel HS, Kraus MF, Filley CM, Anderson CA, Arciniegas DB (2011) Diffusion tensor imaging in mild traumatic brain injury litigation. J Am Acad Psychiatry Law 39:511–523